Response and residual curvature of bent-stretched circular rods with applications to metal forming: closed-form solutions for elastic-perfectly plastic and hyperbolic hardening materials

Alessandra Bonfanti, Stavros Syngellakis, Atul Bhaskar

www.elsevier.com/locate/ijmecsci

PII: S0020-7403(16)30968-7
DOI: http://dx.doi.org/10.1016/j.ijmecsci.2016.12.001
Reference: MS3513

To appear in: *International Journal of Mechanical Sciences*

Received date: 12 April 2016
Revised date: 24 October 2016
Accepted date: 1 December 2016

Cite this article as: Alessandra Bonfanti, Stavros Syngellakis and Atul Bhaskar Response and residual curvature of bent-stretched circular rods with application to metal forming: closed-form solutions for elastic-perfectly plastic and hyperbolic hardening materials, *International Journal of Mechanical Sciences* http://dx.doi.org/10.1016/j.ijmecsci.2016.12.001

Response and residual curvature of bent-stretched circular rods with applications to metal forming: closed-form solutions for elastic-perfectly plastic and hyperbolic hardening materials

Alessandra Bonfanti[a], Stavros Syngellakis[a,b], Atul Bhaskar[a]

[a] *Faculty of Engineering and the Environment, Boldrewood Innovation Campus, University of Southampton, SO16 7QF, Southampton, UK*
[b] *Wessex Institute of Technology, Ashurst Lodge, Ashurst, SO40 7AA, Southampton, UK*

Abstract

Here we develop an analytical expression for the curvature of rods of circular cross-section, when subjected to combined bending and axial force. Small deformations are assumed here so that the deflections are small compared to the cross-sectional dimensions. An enhanced material constitutive law having a linear elastic part followed by smoothly matched hyperbolic hardening is proposed. Analysis for two material models are presented which includes elastic-perfectly plastic material as well as hardening. The effects of the axial force on the response and springback are analytically assessed. The analysis is then applied to the bending of rods of circular cross-section. The analytical results are in excellent agreement with numerical calculations.

Keywords: Rods of circular cross section, elasto-plastic analysis, recoil, hyperbolic hardening, combined bending-stretching

1. Introduction

Plastic deformation of rods is encountered in the manufacture of many components used in automotive, aerospace and transportation engineering sectors of the industry. Perhaps the most common example is forming of metal sheets and curved beams. Such components and processes are used in several mechanical engineering applications, such as load-bearing devices, steel wires for tyre manufacture or in civil engineering structures for aesthetic purposes. The most common cross-section shapes of rods encountered

in engineering are rectangular and circular. The problem of plastic deformation of rods of rectangular cross-section under combined axial-bending loading was solved analytically by Yu and Johnson (1982) sometime ago. Surprisingly, the case of elasto-plastic response and recoil of rods of circular cross-section under combined loading seems missing in the literature. This situation is frequently encountered in metal forming. In addition to such manufacturing technique, a problem having very similar features, in terms of the mechanics and the geometry, also arises in dealing with the micromechanics of many additively manufactured lattice materials such as those for biomedical implants. This is particularly true when fused deposition modelling (FDM) is the manufacturing process. This is because the material is dispensed as stacked cylinders from a circular nozzle. When such biomedical scaffolds undergo complex loading, individual filaments are often under combined stretching and bending. The present work is inspired by a host of such practical engineering problems. The application is however restricted here to the stretch-bending of a single rod.

Analytical prediction of the final manufactured shape after a process such as die-forming is challenging due to the nonlinearities introduced by plasticity and the recovery of the elastic deformation upon unloading. Die geometry frequently dictates the presence of combined axial-bending loading. During the manufacturing process, the material undergoes elastic deformation first, which is followed by plasticity. Due to recoverable elastic deformation, the final shape of the object, following the forming process, is not the one imposed by the forming tool, but the recoverable elastic strain must be deducted. Several possible measures are taken in practice to account for the springback. For example, extra features in radii or variation in blank holder force are used to ensure the shape of the formed part to be the same as intended after springback has taken place. In stretch-bending processes, rods are clamped and stretched from its ends and bent over a die (El-Domiaty and Elsharkawy (1998)). The key problem encountered is the control of the effective residual curvature after the process. The application of a tensile load reduces the springback; however, the inevitable elastic recovery will always be observed which necessitates studies to quantitatively predict the same. Trial and error methods have often been used to establish the appropriate setting parameters. Researchers have also looked at the influence of cross-section shape (Miller et al. (2001); El-Domiaty and Elsharkawy (1998)), material and loading parameters on the final deformed shape (Zhao et al. (2013)). Xu et al. (1987) analysed L-beams for elasto-plastic response and springback while ac-

counting for the shift and the rotation of the neutral axis. To the best of our knowledge, the commonly encountered problem of simultaneously bent-stretched circular rods and wires has not been solved in a closed-form yet.

Another motivation of the present work is a closely related problem of the elasto-plastic response and recoil of lattice structures. Such architectures are often used for biomedical implants where porosity is intended to facilitate cell adhesion and growth. The high energy absorption capability (Dharmasena et al. (2008), Wadley et al. (2008)) as well as heat transfer characteristics (Tian et al. (2004), Tian et al. (2007)) make them also suitable materials for automotive catalytic converters or impact and sound absorption devices (Gibson and Ashby (1999), Tuncer (2005)), for example. The possibility to manufacture such lattice material in a controlled fashion-unlike foams having random pore geometry-is greatly enhanced by the advent of additive manufacturing (Yang et al. (2001), Yang et al. (2002)). Coupled with the ability to predict the structural response and be able to design material with required properties, the future of structured porous solids is very promising. The apparent response of such structures can be inferred from that of a single strut. Such analyses for lattice structures were carried out for elastic response by Gibson et al. (1982) and Bonfanti and Bhaskar (2015) for elasto-plastic response and recoil. Coupled with the naturally circular shape of filaments found in lattice structures manufactured using Fused Deposition Modelling (FDM), the importance of the mechanical response of a single circular rod under complex loading involving axial and bending deformations becomes critical for micro-mechanical analyses.

Approaches to predict elasto-plastic response and recoil of elastic rods make use of various approximations in order to simplify analysis (Johnson and Mellor (1983); Kaliszky (1989); Rees (2006); Chakrabarty (2006)). The situation is particularly complicated when the stress-strain relationship in the plastic regime is complex. Therefore, analytical results for elasto-plastic beam response are limited. Due to analytical difficulties in solving the equation governing the elasto-plastic problem, numerical and experimental techniques have been extensively used in the past (Saje et al. (1998); Mines and Jones (1995)). However, some closed form solutions are also available. Exact solutions are known for a beam with rectangular cross-section subjected to constant bending moment and only few for non-constant bending moment distributions along the length, such as linear (Yu and Johnson (1982)) or quadratic (Chakrabarty (2006); Prager and Hodge (1951); Štok and Halilovič (2009)) have been studied. In all these analyses, elastic-perfectly plastic material has

been assumed. This idealisation is frequently used in analytical work as the starting point, since it simplifies the mathematics and includes all the essential features of the plasticity problem. In order to obtain a more realistic description of the beam behaviour, the non-linear hardening effect must be taken into account during the plastic analysis. The present study provides such a generalisation and yet successfully affords closed form solution.

A theoretical study on the nonlinear bending of wires with rectangular and circular cross section assuming three different types of material behaviour was presented by Baragetti (2006). They developed an analytical approach to predict the final shape of a wire without using finite element analysis. A well-known geometry that has attracted attention with regards to bending processes is the tube, widely used in the aircraft industry. Theoretical studies of elasto-plastic bending of tubes are available in the literature to predict their final deformed shape and springback (Al-Qureshi (1999)). In many engineering applications, the beam is subjected to combined bending and tensile axial force. The application of a longitudinal force affects the position of the neutral axis; therefore, the stress distribution in each cross-section is not symmetric even if the cross-section is geometrically symmetric with respect to the such axis. Yu and Johnson (1982) presented the first theoretical study for a beam with a rectangular cross-section, made of an elastic-perfectly plastic material under combined bending and axial force. *However, to our knowledge, analytical solutions for other geometries, including circular cross-section, are not available for combined loading.* A source of mathematical difficulty under combined loading is the lack of validity of the superposition principle because of the non-linearity introduced to the problem by plasticity.

Several mathematical representations are available to model material hardening. Power law is one of the most commonly used material constitutive law when the plastic strain is large (Samuel (2006); Dafalias and Popov (1975)). However, this representation introduces difficulties in the analysis. A new mathematical model which captures both linear and nonlinear behaviour is proposed here. This model is amenable to analysis as presented in Section 2. The present work aims to provide an analytical calculation of the elasto-plastic deformation and recoil of a thin beam of circular cross-section for two different material laws (a) elastic-perfectly plastic and, (b) with the model of hyperbolic hardening introduced here. The diameter is assumed to be much smaller than the length of the beam allowing neglecting the shear deformation through the cross-section.

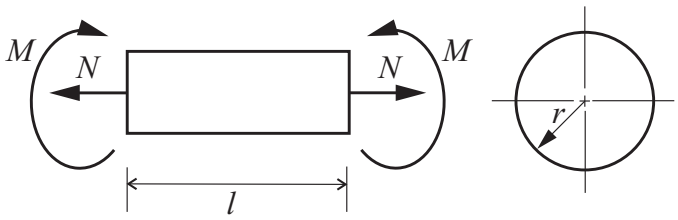

Figure 1: Initial straight beam of circular cross section loaded with axial force N and bending moment M.

The paper is organized as follows. In Section 2, the plastic analysis of a beam under combined loading is described. Further the constitutive model with hyperbolic hardening is introduced here which allows smooth transition at an yield point from linear elastic to non-linear hardening. The development of the analytical model assuming an elastic-perfectly plastic material is presented in Section 2.1. Section 2.2 takes up the analysis assuming the hyperbolic nonlinear model. Following this, the calculation of springback upon removal of external load is presented in Section 2.3. The load-curvature relationships for a rod undergoing metal forming under axial and transverse forces is described in Section 3. The presence of combined loading is a result of the geometry of the punch-die system. Finally, concluding remarks are made in Section 4.

2. Plastic analysis and springback of beams under combined axial and bending loading

An initially straight beam of circular cross section of radius r is loaded by a constant bending moment M and a tensile force N, as shown in figure 1. Small deformations are assumed here so that the deflection of the beam is small compared to the cross-sectional dimensions. Also, it is assumed that the cross-section of the beam remains plane during the elasto-plastic deformation (Bernoulli's hypothesis). As a result, strain is linearly related to the distance from the neutral axis. The beam is also assumed stress-free before loading.

For different combinations of M and N, the stress distribution over a cross section can be one of the three types:

1. Wholly elastic stress distribution: no fibre parallel to the longitudinal axis of the beam undergoes plastic deformation;

2. Primary plastic stress distribution: only part of one side of the beam, either above or below the neutral axis, is plastically deformed;
3. Secondary plastic stress distribution: the cross-section is partially plastically deformed above and below the neutral axis. However, the extent of the two plastic zones is asymmetric due to the presence of axial load.

An ideal elastic-perfectly plastic material model is considered first. The study is then extended for an elasto-plastic material model with nonlinear hardening. The following dimensionless variables for axial force, moment and curvature of the section are now defined as

$$n = |N|/(\sigma_y r^2), \quad m = |M|/(\sigma_y r^3) \quad \text{and} \quad \phi = |\kappa|/\kappa_e, \tag{1}$$

where σ_y is the yield stress, r is the radius of the cross section and κ_e is the initial yield quantity under pure bending for the curvature given by

$$\kappa_e = \sigma_y/(rE), \tag{2}$$

where E is the Young's modulus.

2.1. Elastic-perfectly plastic material behaviour

Consider isotropic and homogeneous material that exhibits elastic-perfectly plastic behaviour so that the stress-strain relationship can be expressed as

$$\sigma = \begin{cases} E\epsilon & \sigma < \sigma_y \\ \sigma_y & \sigma \geq \sigma_y \end{cases}. \tag{3}$$

For a combination of M and N, the stress distribution over each cross section can be qualitatively classified in one of the three categories listed before. By setting up the equations for force and moment equilibrium for each category, the load-curvature relationship is derived in the following analysis.

2.1.1. Elastic-perfectly plastic material: the elastic regime E_r

In this regime, the deformation is purely elastic; therefore, the final stress distribution is obtained by superposing the effects of separately applied axial force and bending moment. Note that under this loading state the longitudinal axis of the beam and the longitudinal axis through the centroid of the cross-section do not coincide, in contrast to the pure bending case normally studied.

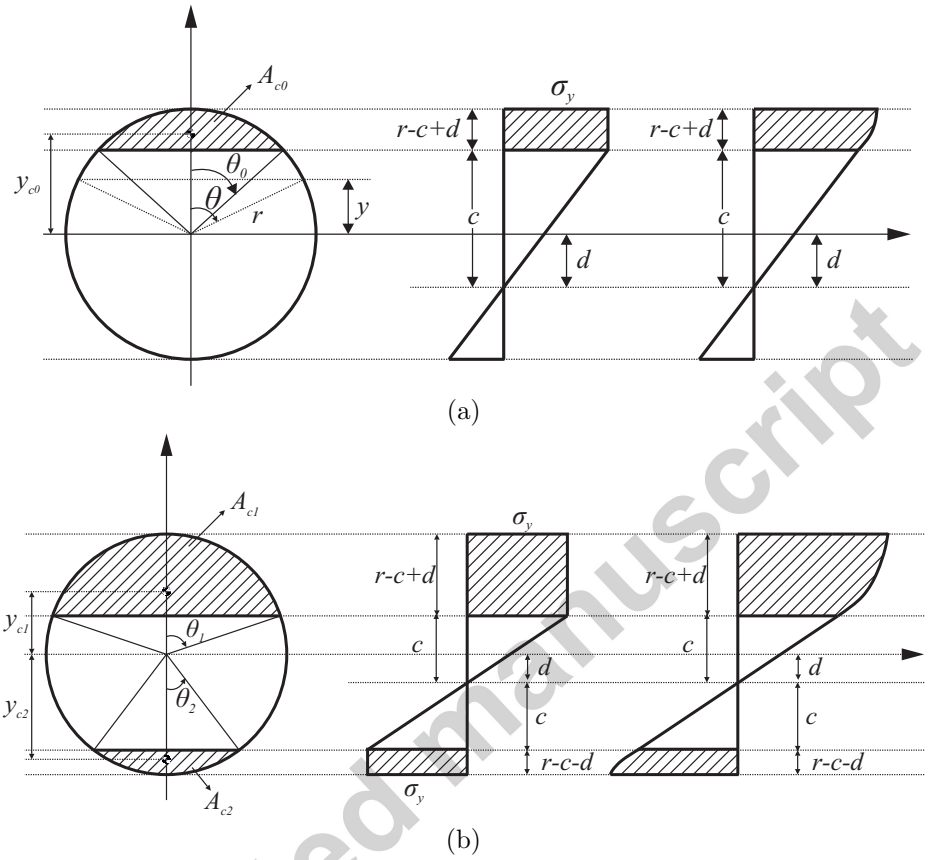

Figure 2: (a) Stress distribution across the circular cross section: PI regime. The circular segment area is denoted by A_{c0} and the location of its centroid by y_{c0}.(b) Stress distribution across the circular cross section: PII regime. The circular segment areas are denoted by A_{ci} and the location of its centroid by y_{ci}. Stress profiles for elastic-perfectly plastic case are shown at the centre and these for hyperbolic hardening at the right end.

Using of the superposition principle, it can be shown that the load-curvature relationship in the elastic regime is

$$\phi = m \tag{4}$$

for $m + n \leq 1$. Hence, the boundary of the onset of plasticity for this regime is $m + n = 1$, beyond which the treatment must account for plasticity.

2.1.2. Elastic-perfectly plastic material: the primary plastic regime PI

Due to the asymmetric stress distribution above and below the line passing through the centroid on the cross-section, upon simultaneous application of N and M, one side of the beam undergoes plastic deformation as loading is increased. This is shown in figure 2 (a). The non-linearity of the problem introduced by yielding now prohibits the use of the superposition principle. Therefore, the load-curvature relationship can only be calculated by imposing the force and moment static equilibrium conditions at the cross section.

The cross-section is assumed to be circular having radius r in which a circular segment of area A_{c0} has undergone plastic deformation. The central figure within 2 (a) refers to the stress profile for PI regime when elastic-perfectly plastic stress-strain relationship is used. Let θ_0 be half of the central angle of the circular segment in radians and y_{c0} the position of its centroid respect to the centre of the circle. The position along the circumference is described using the angle θ, measured from the vertical axis. It turns out that parametrising the plastic zone in the polar co-ordinates using θ_0 facilitates calculations greatly.

Static equilibrium of the axial force over the cross-section leads to

$$\left(\theta_0 - \frac{1}{2}\sin 2\theta_0\right) - \frac{2}{c}\left[\frac{r}{3}\sin^3\theta_0 + \frac{d}{2}\left(\theta_0 - \frac{1}{2}\sin 2\theta_0\right) - \pi\frac{d}{2}\right] = n, \qquad (5)$$

where d is the shift of the neutral axis from the centre of the section and c is the distance of the first yielded fibre from the neutral axis (figure 2 a). Equilibrium of the bending moment due to stress distribution over the cross-section results in

$$\frac{2}{3}\sin^3\theta_0 - \frac{2}{c}\left[\frac{d}{3}\sin^3\theta_0 + \frac{r}{8}\left(\theta_0 - \frac{1}{4}\sin 4\theta_0\right) - \pi\frac{r}{8}\right] = m. \qquad (6)$$

A detailed derivation of this can be found in the Appendix.

Substituting from

$$(c-d)/r = \cos\theta_0 \qquad (7)$$

for d into equations (5) and (6), we obtain a pair of simultaneous equations

$$\begin{array}{c} \left(\pi - \theta_0 + \frac{1}{2}\sin 2\theta_0\right) + \frac{2}{3}\sin^3\theta_0 = (\pi - n)\,\frac{c}{r} \\ \frac{1}{4}\left(\pi - \theta_0 + \frac{1}{4}\sin 4\theta_0\right) + \frac{2}{3}\cos\theta_0\sin^3\theta_0 = m\frac{c}{r}. \end{array} \qquad (8)$$

in variables θ_0 and c/r. The unknown c/r can be eliminated leading to a single equation in terms of θ_0 only. Substituting this into one of the equation in (8), we determine the value of c. Once the value of c is known, then the dimensionless curvature ϕ can be calculated from

$$\phi = r/c. \tag{9}$$

2.1.3. Elastic-perfectly plastic material: the secondary plastic regime PII

When the axial force and bending moment, N and M respectively, are further increased, both sides of the beam undergo plastic deformation, as shown in figure 2 (b). As for the case of primary plastic regime, the load-curvature relationship is found by imposing the static equilibrium since the nonlinearity due to plasticity forbids the application of the superposition principle.

When plastic deformation develops on both sides of the longitudinal axis, the two yielded segments have a different area, A_{c1} and A_{c2} above and below the neutral axis respectively, because of the asymmetric distribution respect the centre of the section. The locations of the centroids of the plastic regions are, respectively, y_{c1} and y_{c2} and the central angles of the two plastic regions are θ_1 and θ_2, as shown in figure 2 (b). The central figure within 2 (b) refers to the stress profile for PII regime when elastic-perfectly plastic stress-strain relationship is used.

The axial force equilibrium now requires summing contributions from the two outer plastic regions and the elastic core. The result is expressed as

$$\left(\theta_1 - \frac{1}{2}\sin 2\theta_1\right) - \left(\theta_2 - \frac{1}{2}\sin 2\theta_2\right) - \frac{4}{3}\frac{\sin^3\theta_1 - \sin^3\theta_2}{\cos\theta_1 + \cos\theta_2} + \frac{\cos\theta_1 - \cos\theta_2}{\cos\theta_1 + \cos\theta_2}(\pi - \theta_1 - \theta_2) + \\ + \frac{1}{2}\sin 2\theta_1 + \frac{1}{2}\sin 2\theta_2 = n. \tag{10}$$

Similarly, the moment equilibrium now requires integrating contributions over the cross-section leading to

$$\frac{2}{3}\left(\sin^3\theta_1 + \sin^3\theta_2\right) - \frac{2}{3}\frac{\cos\theta_1 - \cos\theta_2}{\cos\theta_1 + \cos\theta_2}\left(\sin^3\theta_1 - \sin^3\theta_2\right) + \\ + \frac{1}{8}\frac{1}{\cos\theta_1 + \cos\theta_2}\left[-4\left(\theta_1 + \theta_2 - \pi\right) + \sin 4\theta_1 + \sin 4\theta_2\right] = m. \tag{11}$$

A detailed derivation of (10) and (11) is presented in the Appendix. Equations (10) and (11) constitute a nonlinear system of algebraic equations that cannot be reduced further. From the values of θ_1 and θ_2 obtained, the distance c of the fibre first yielded from the neutral axis is obtained as

$$c = r/\left[2(\cos\theta_1 + \cos\theta_2)\right], \tag{12}$$

from which the curvature is derived using equation (9).

2.2. Hyperbolic hardening model

Engineering design requires realistic constitutive models that relate stress and strain within materials. Mathematical description of constitutive behaviour frequently requires a compromise between realism and complexity of the model for the given purpose. The classic plasticity theory developed from the study of metals and other crystalline materials. At microscopic level crystal planes slip in the direction of the largest shear stress. This slip is possible because of the motion of dislocations of atom planes. The two commonly used mathematical descriptions employed to model the macroscopic hardening behaviour of materials are Hollomon's equation and Ludwik's equation (Samuel (2006)). Since these power law expressions introduce mathematical difficulties in the plastic beam bending analysis and also lack a linear elastic regime, a new mathematical representation of the stress-strain curve is sought here. A very wide range of engineering material show a linear response for low strain followed by a plastic region of hardening where the tangent modulus of the material monotonically reduces upon increased strain. Inspired by the constitutive law used for soil and polystyrene geofoam (Chun et al. (2004)), a linear model followed by an hyperbolic stress-strain relationship has been proposed here (figure 3). The stress-strain behaviour of several materials can be separated into the linear elastic behaviour and the nonlinear behaviour due to plasticity. The linear behaviour is observed until the yield point is reached and it is modelled using a straight line which passes through the origin and whose slope is the Young's modulus. The plastic behaviour is described here by a rectangular hyperbola with asymptotes translated with respect to the reference system. The proposed constitutive relation is written

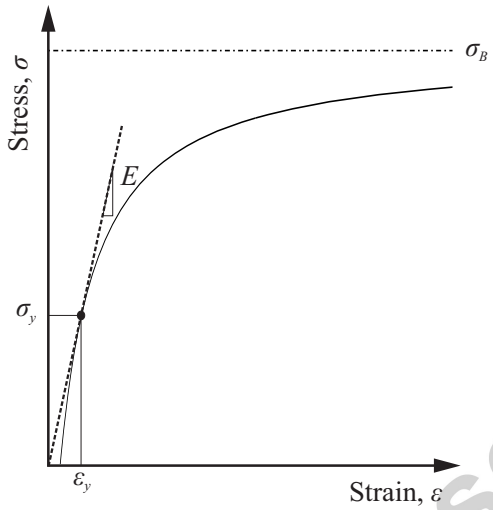

Figure 3: Proposed stress-strain relationship with hyperbolic hardening

as

$$\sigma = \begin{cases} E\epsilon & \sigma < \sigma_y \\ \dfrac{B\epsilon + D}{A - \epsilon} & \sigma \geq \sigma_y \end{cases}. \tag{13}$$

where A, B and D are the coefficients of the hyperbola and $\sigma = -B$ and $\epsilon = A$ are the asymptotes. The parameters are calculated by imposing the continuity and differentiability at the interface of the elastic and the plastic regimes. The first requirement is expressed as

$$\sigma(\epsilon = \epsilon_y) = \sigma_y. \tag{14}$$

The gradient continuity between the hyperbola and the straight line at the yield point provides a second condition

$$\left.\frac{\mathrm{d}\sigma}{\mathrm{d}\epsilon}\right|_{\epsilon=\epsilon_y} = E. \tag{15}$$

The material parameters most readily available from the experiments are the Young's modulus E, yield stress σ_y, yield strain ϵ_y and the parameter B which is the σ asymptote. To test how realistic the proposed hyperbolic

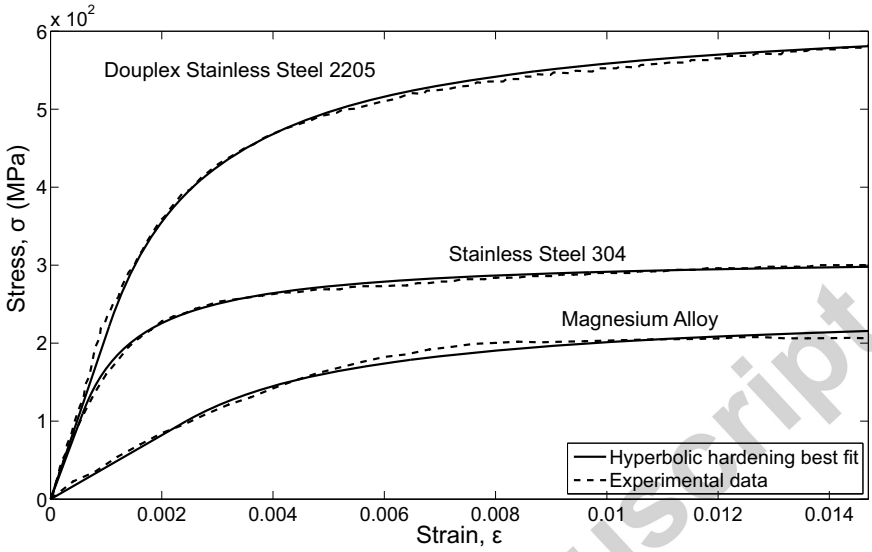

Figure 4: Hyperbolic interpolation for Douplex stainless steel 2205, Stainless steel 304 and Magnesium alloy (Original data from Association (nd); Fare et al. (2010)).

Material	A (10^{-4})	B (MPa)	D (MPa)
Douplex Stainless Steel 2205	-8.98	-6.32×10^2	2.34×10^{-1}
Stainless Steel 304	-4.84	-3.12×10^2	6.37×10^{-2}
Magnesium Alloy	-0.122	-2.50×10^2	2.44×10^{-1}
Elastic-perfectly plastic	-0.111	-2.20×10^2	2.32×10^{-2}

Table 1: Hyperbola coefficients obtained from the genetic algorithm for the real materials shown in figure 4 and the ideal elasto-perfectly plastic material.

hardening model is, here we compare the best fit to experimentally obtained data (Association (nd); Fare et al. (2010)). For this, the difference between the data and the model was treated as error to facilitate curve fitting. The sum of square of the error was minimised by the use of a Genetic Algorithm (GA). The process of curve-fitting was thus treated as an error minimisation problem by a GA. The $\sigma - \epsilon$ relationship (13) was fit to previously published data for three different real materials (figure 4). The hyperbola parameters estimated for the set of trial materials shown in the figure are summarized in Table 1.

The experimental data and the hyperbolic hardening model are found to be in good agreement. Note that a somewhat similar representation has been

recently used for cast iron (Rajani (2012)). There, the hyperbolic model has been used to describe the whole constitutive material law because the cast iron shows non-linearities also at low stresses. Unlike Rajani (2012), the model proposed here has a linear part which simulates many real material behaviour more faithfully.

The analysis for the elastic-perfectly plastic material in the three regimes of plasticity (on the lines of Section *2.1*) is now carried out for the hyperbolic hardening model.

2.2.1. Hyperbolic hardening: the elastic regime E_r

The stress distribution over the cross-section remains the same as that discussed previously in Section *2.1* for the elastic-perfectly plastic case. Therefore, all the relationships developed there stay unchanged.

2.2.2. Hyperbolic hardening: the primary plastic regime PI

When a cross section starts yielding under combined axial loading and flexure, the plastic deformation takes place only on one side of the beam as for the elastic-perfectly plastic material. The presence of the axial force shifts the neutral axis away from the centroid, causing an asymmetric stress distribution whose qualitative behaviour is illustrated in figure 2 (a). The stress profile for hyperbolic hardening is shown in the right figure within 2 (a). Whilst for the elastic-perfectly plastic material model the maximum stress remains constant, once the yield stress σ_y is reached, for the hyperbolic hardening material, the post-yielding stress distribution is nonlinear and requires new analysis.

Johnson and Mellor (1983) presented the stress distribution over each cross section by re-drawing the material stress-strain diagram from the neutral line. Therefore, the shape of the nonlinear stress profile is known. By using this argument, the axial force equilibrium yields

$$\sigma_y \int_{\theta_0}^{0} 2\sigma(\theta) \sin^2\theta d\theta - \frac{2}{c} \int_{\pi}^{\theta_0} (r\cos\theta + d) \sin^2\theta d\theta = n \tag{16}$$

and similarly the moment equilibrium results in

$$\sigma_y \int_{\theta_0}^{0} \sigma(\theta) 2\sin^2\theta \cos\theta d\theta - \frac{2}{c} \int_{\pi}^{\theta_0} (r\cos\theta + d) \sin^2\theta \cos\theta d\theta = m \tag{17}$$

where

$$\sigma(\theta) = \frac{B(\epsilon_y/c)(r\cos\theta + d) + D}{A - (\epsilon_y/c)(r\cos\theta + d)}. \tag{18}$$

The first integral in equation (16) and (17) is the contribution of the stress over the circular segment having undergone plastic deformation, whilst the second integral is that corresponding to the area where the deformation is still elastic. A detailed derivation of $\sigma(\theta)$ is presented in the Appendix. The three unknowns c, d and θ_0 are related by equation (7). By substituting one variable from equation (7) into (16) and (17), a system of two equations in two unknowns is obtained. The nondimensional curvature is finally calculated using equation (9). The curvature relation can be integrated to determine the transverse deflection.

2.2.3. Hyperbolic hardening: the secondary plastic regime PII

Increasing N and M further leads to plastic deformation on both sides of the beam as shown in figure 2 (b). The corresponding stress profile for the hyperbolic hardening model is shown in the right figure of 2 (b) In a manner similar to that applied for the PI case, the stress profile after yielding shows a nonlinear behaviour. In the current model, the hyperbolic function introduced here is used to describe the post-yield stress distribution.

The equilibrium along the axial direction can be expressed as

$$\int_{\theta_1}^{0} \sigma(\theta) 2\sin^2\theta d\theta + \int_{\theta_2}^{0} -\sigma(\theta) 2\sin^2\theta d\theta - \frac{2}{c}\int_{\pi}^{\theta} (r\cos\theta + d)\sin^2\theta d\theta = n. \tag{19}$$

which is obtained by summing the contributions of fibres under tension and compression over the circular cross-section. Similarly, moment equilibrium leads to

$$\int_{\theta_1}^{0} \sigma(\theta) 2\sin^2\theta\cos\theta d\theta + \int_{\theta_2}^{0} -\sigma(\theta) 2\sin^2\theta\cos\theta d\theta - \frac{2}{c}\int_{\pi}^{\theta} (r\cos\theta + d)\sin^2\theta\cos\theta d\theta = m, \tag{20}$$

where the moment over the cross-section is calculated via the sum of the integrals above. The first two integrals are the stress contributions from the upper and lower circular segment undergone plastic deformation, whilst the

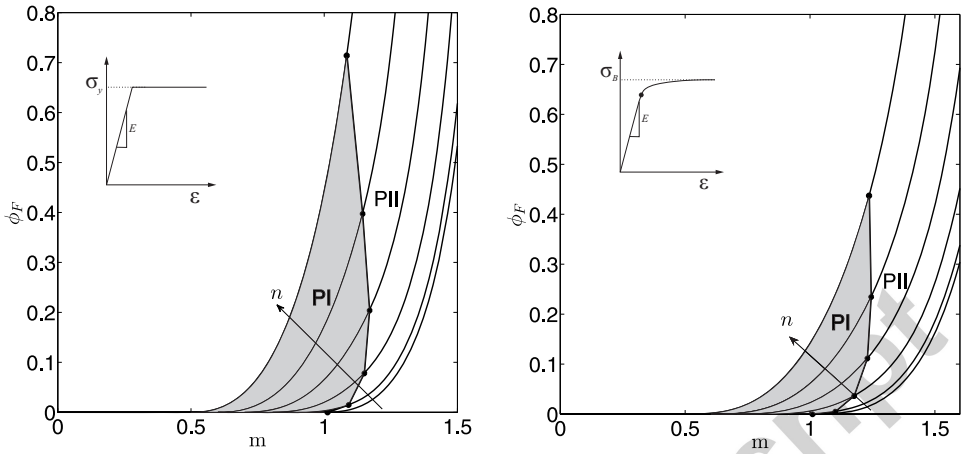

Figure 5: Non-dimensional curvature after the unloading for different combinations of m and n. The non-dimensional axial force, n, is 0.0, 0.1, 0.2, 0.3, 0.4 and 0.5, respectively from the right to the left lines. The primary plastic region and the secondary plastic region are demarcated by the dark solid lines. (a) Elastic-perfectly plastic material ($E = 209$ GPa, $\sigma_y = 240$ MPa) (b) Hyperbolic hardening material ($E = 209$ GPa, $\sigma_B = 240$ MPa), yielding for this occurs at 200 MPa shown by a dot.

last integral is attributed to the area under elastic deformation. A nonlinear system of two equations, (19) and (20), involving four unknowns c, d, θ_1, θ_2 is obtained. Two further conditions that relate these four unknowns are given by $\cos\theta_1 = (c-d)/r$ and $\cos\theta_2 = (c+d)/r$. Finally we have a pair of non-linear algebraic equations in terms of two unknowns which can be solved.

2.3. Springback of a beam following simultaneous application of bending moment and axial force

When the applied moment M and axial force N are removed, the elastic deformation is recovered but the plastic deformation remains permanently within the material. If the unloading is assumed to be linearly elastic, the final residual non-dimensional curvature is given by

$$\phi^F = \phi - m. \tag{21}$$

For all combinations of bending moment and axial force, the expression above provides the springback.

The numerical results for the elastic-perfectly plastic material and a material showing hyperbolic hardening, whose horizontal asymptote σ_B corresponds to the yield stress of the elastic-perfectly plastic material, are plotted in figure 5. For the same combination of m and n, the final curvature ϕ_F is lower for the material showing nonlinear hardening. The shaded regions show the combination of normalised axial force and bending moment that lead to primary plastic state of stress. Figure 5(a) relates to elastic-perfectly plastic case whereas 5(b) to hyperbolic hardening. When an elastic-perfectly plastic material undergoes plastic deformation, the hardening rate (measured by the tangent modulus) is equal to zero. Thus, the plastically deformed material no longer resists if any additional strain is applied. By contrast, to further deform a material showing an hardening rate different from zero, an increasing stress is required.

3. An illustrative example: press-brake bending of a metal rods

The results obtained in Section 2 can now be applied to calculate elasto-plastic response for practical manufacturing processes. Consider a press-brake bending of a metal rod, as shown in figure 6 (a). Observed the symmetry of the problem, half of the rod can be modelled as a cantilever beam. Here the bending moment varies along the length of the beam and an axial force is applied additionally. The rod is of circular cross section with radius r, clamped at one end and subjected to a concentrated force F at the tip inclined at an angle α, as shown in figure 6 (b). The inclination of the reaction from the die is a consequence of the direction of the normal to the die surface. Thus the geometry of the problem enforces simultaneous presence of significant axial force and bending moment. The inclined load can be separated in its transverse and axial components, which are respectively P and N (see figure 6 b). The plastic zone is depicted by the hatched area in the figure and it shows asymmetric distribution due to the presence of axial force. Note that tensile or compressive N results in the same final curvature because both tend to the same departure in stress distribution form the elastic case but on the opposite sides of the centre line. The extent of plasticity on the top fibre is given by $0 \leq x \leq x_1$ and that for the bottom fibre by $0 \leq x \leq x_2$. PI regime spans $x_1 \leq x \leq x_2$ and PII regime spans $0 \leq x \leq x_1$. Finally, $x_2 \leq x \leq l$ corresponds to the elastic part of the structure.

Two cases of the material behaviour are considered: that of elastic-perfectly plastic and the one with hyperbolic hardening. To simplify the

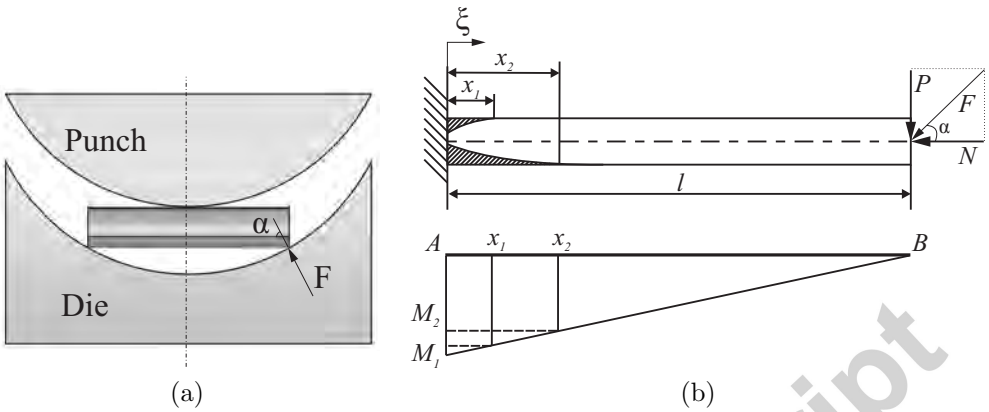

Figure 6: (a) Press-brake bending of a metal rod (b) Half of the work piece modelled as a cantilever beam with axial and shear components. The hatched areas are the plastic zones that spread along the beam while the load is increased. Due to the asymmetric stress distribution, the two sides of the beam do not undergo plastic deformation at the same time. Moment distribution along the beam due to the shear force P.

analysis, the maximum bending moment at the root of the beam is expressed in the following non-dimensional form

$$m^* = Pl/(\sigma_y r^3). \tag{22}$$

where $\sigma_y r^3$ is the factor of dimensionalisation; l is the length of the beam. Introduce the non-dimensional co-ordinate ξ along the beam and the non-dimensional transverse deflection η as $\xi = x/l$ and $\eta = wrE/(l^2\sigma_y)$, where w is the beam deflection. The non-dimensional curvature is now given by

$$\frac{\mathrm{d}^2\eta}{\mathrm{d}\xi^2} = \phi. \tag{23}$$

The complete beam deflection is obtained by integrating the curvature expressions derived in the previous sections, and applying the geometric boundary conditions at the fixed end

$$\eta = 0 \quad \text{and} \quad \frac{\mathrm{d}\eta}{\mathrm{d}\xi} = 0 \quad \text{at} \quad \xi = 0. \tag{24}$$

The final deflected shape of the cantilever beam after the unloading is found

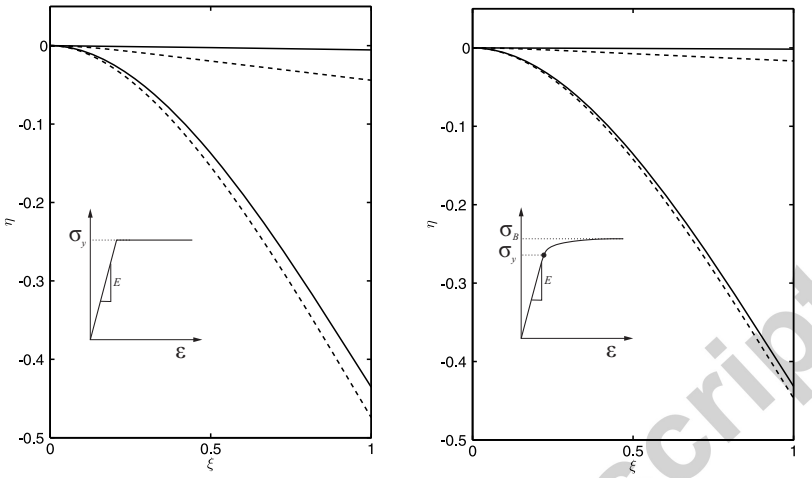

Figure 7: Deflection of the cantilever beam with circular cross section. The results are presented for both elastic-perfectly plastic materialand elasto-plastic material with hyperbolic hardening. Different combinations of n and m^* are examined to study the influence of the axial force on the deformed shape: the solid line refers to $n = 0.0$ and $m^* = 1.3$, whilst the dashed line to $n = 0.3$ and $m^* = 1.3$.

by subtracting the elastic deflection from the expression of η:

$$\eta_F = \eta - m^*(1 - \xi). \tag{25}$$

Two loading conditions were considered. The first assumes a cantilever beam subjected to pure bending, while the second example considers a cantilever beam subjected to a combined loading: bending moment and axial force. The deformed shapes are presented in figure 7. As expected, for the same loading state, the deflection obtained using an elasto-plastic material with nonlinear hardening is lower. This is due to the increased strength of the material attributed to the strain hardening. A smaller elastic recoil is observed when an axial force is applied. In manufacturing processes, like metal forming, the estimation of the elastic recoil is fundamental in determining the load to which the solid must be subjected so that the desired final shape is obtained.

The results obtained using the analytical model are compared here against those obtained using a finite element approximation. The analysis has been performed using the Finite Element Analysis commercial code Abaqus. The

cantilever beam is discretised using the beam element B23, which does not allow for shear deformation, but it has stretch degrees-of-freedom. The beam is fixed at left end and it is loaded by prescribing a compressive axial force and shear force at the right end. The analytical and computational results are in good agreement, as shown in figure 8 (dashed lines). The application of the axial force results in the shift of the neutral axis and axial strain. The analytical model takes into consideration only the change of position of the neutral axis; therefore, the slight difference between analytical and FEM results can be attributed to the absence of the stretch in the model earlier developed.

Although, neglecting geometric non-linearity might appear as a limitation, it enables us to successfully develop a new simple and accurate *analytical* solution to predict and control the stretch-bending final deformed shape and springback of rods and beams in traditional manufacturing processes. This is valuable for assigning the process parameters as opposed to current practice of applying a combination of experience, trail-and-error approaches, or detailed computations that provided result for specific geometries without any analytical information about the sensitivity to the parameters. In practice, metal forming processes include both geometric and material nonlinearities. The nonlinear material behaviour is likely to be much more significant; therefore, in order to handle the problem analytically, we considered the influence of the material nonlinearities only while neglecting the nonlinear term arising from the large displacement as a first approximation. We study these effects in the next section.

3.1. The effects of geometric nonlinearity and kinematic hardening

The analysis presented above is restricted to small strains. Thus, only the effects of the material nonlinearity were included. We lift the restrictions of geometric linearity and kinematic hardening now and include geometric non-linearity in our calculations first.

We can assess the role of geometric nonlineariy on the elasto-plastic response computationally. We carried out finite element calculations with and without the effects of geometric non-linearity while always accounting for plasticity. The deflected shape that includes the effects of large deformations and large displacements obtained from finite element calculations using the commercial software Abaqus is presented in figure 8. The two deformed shapes obtained using FEM–with and without geometric nonlinearity, show

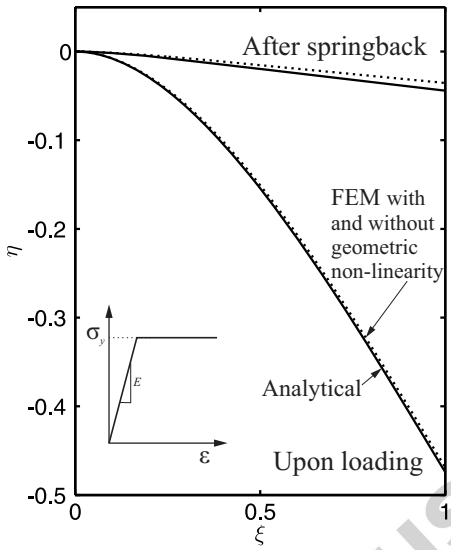

Figure 8: Comparison of the elasto-plastic deformed shape and springback obtained using the analytical model (solid lines–with and without geometric nonlinearity) developed here and the commercial Finite Element software Abaqus (dashed lines) for $m^* = 1.3$ and $n = 0.3$.

excellent agreement. This illustrates that the geometric nonlinearity is of minor importance for slender beams and small deformation.

In the prediction of springback, both kinematic hardening and plastic anisotropy play important roles. However, the reduction in stiffness during the plastic deformation, due to the Bauschinger effect, is important when *several cycles of stress past plasticity* are applied. Here, we are concerned with applications where the structure undergoes only one cycle of stress reversal. This is a common scenario in metal forming. Likewise, in situations such as the analysis of cardiovascular stents during expansion, a single cycle of springback is of interest. This is also true in many impact and crash applications when only one cycle of plasticity is applied. Therefore, the Bauschinger effect was neglected, as a first approximation in the previous section, in order to obtain a closed form analytical solution. As demonstrated by Yu and Johnson (1982), under the assumptions made for the analysis, re-yielding cannot occur during unloading if an elastic perfectly plastic material is assumed; therefore, the unloading is fully elastic. This justifies our approach in the previous sections even though a compromise to realism takes place as a results which is deliberate in the interest of developing analytical results. The assessment of

situations where kinematic hardening has an appreciable effect is taken up next.

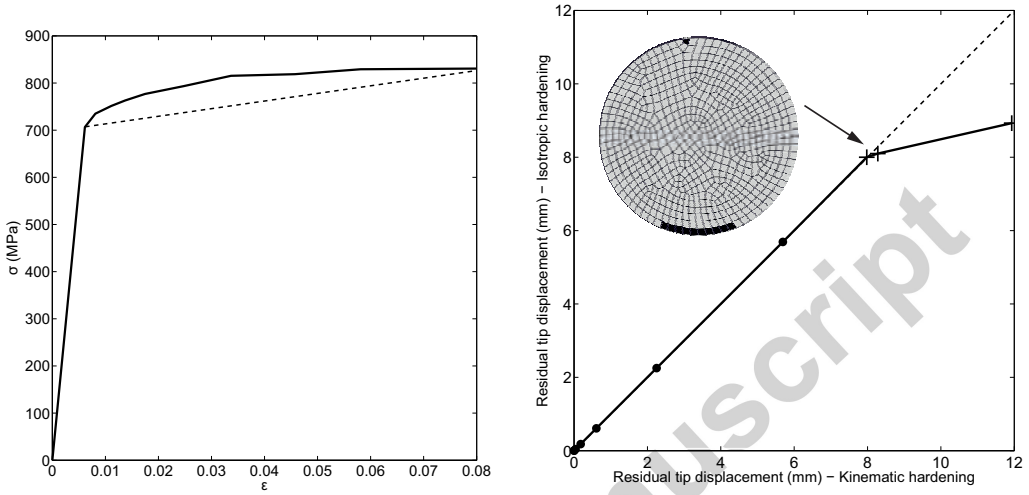

(a) (b)

Figure 9: (a) Constitutive material curve for Douplex UNS31803 alloy. The solid line is the experimental curve Rasmussen (2003), the dashed line is the linear hardening model. (b) Final tip deflection for both kinematic and hyperbolic hardening. Reyileding occurs when high load is applied; this is depicted by the black area within the circular cross-section in the inset. However, the structure fails under such loading–crosses.

The prediction of springback depends mainly on the accuracy of the residual stress calculation, directly related to the material properties, both during loading and unloading. Under the assumption of small strain, we can computationally assess the effects of the kinematic hardening. The material considered here is Douplex UNS31803 alloy (see figure 9 a). The nonlinearity is now modelled by piece-wise linear curves, *both assuming isotropic and kinematic hardening*. The tip deflection after springback is in a good agreement as calculated from the two hardening models (isotropic and kinematic hardening). Results obtained for isotropic hardening assumption are plotted against those computed using kinematic hardening in figure 9 b. The relationship along a line equally inclined to the two axes confirms that the role of kinematic hardening is non-existent for all the points up to ~ 7.5 mm deflection. Reyielding occurs when the force is further increased. The influence of kinematic hardening can be observed in the last two points computed on this graph. The "AC YIELD" state variable within Abaqus (a flag indicating

if the material is currently yielding, or not) is plotted within the clamped cross-section of the rod (see the inset of figure 9 b). The black area is the region that has undergone reyielding *after springback*, whilst the white area is still under pure elastic deformation. This shows that *the volume of the plastic region is negligible* compared to the total volume of the rod indicating the insignificance of kinematic hardening. However, at this stage, the structure fails as the strain within the rod exceeds the maximum strain allowed by the material (denoted by "plus signs" in figure 9 b). This shows that for the case considered here, kinematic hardening has no impact for most cases and the results with or without accounting for this match very well. However, it is also clear that there are circumstances when reyielding could occur significantly, thus affecting the results.

4. Conclusions

Analytical models incorporating the influence of axial force on elasto-plastic bending and springback of beams of circular cross-section were developed. Such an analysis has been previously performed only for a rectangular cross-section with elastic-perfectly plastic constitutive model. This has been possible by the introduction of an improved mathematical description of the stress-strain curve which combines a straight line with a translated rectangular hyperbola. This mathematical representation of the material constitutive law gives us the possibility to exactly calculate the linear-elastic behaviour at low strain in addition to that in the plastic regime. The analysis assumes that plane cross sections remain plane after bending and the deformations are small with respect to the dimensions of the beam.

The model relates the radius of curvature to the combination of bending moment and axial force during the loading and unloading process. The relationship has been expressed using mathematical equations, leading to the exact solution presented here. The analysis developed above enables a designer to chose the correct loading to obtain the desired final shape of the beam during forming processes.

The theoretical model predicts the loading and unloading of a beam with circular cross section for two material models. This allows to assess the deformed shape for most of the available materials. Finally, the methodology developed here is applied to the practical problem of bending of a circular rod within a die where the geometrical necessity forces combined loading. The

results for the two material models have been verified with those obtained from the FEM analysis resulting in an excellent agreement.

The analysis is limited to small deflection and deformation ignoring geometric non-linearity as well as kinematic hardening. A computational assessment of these effects show the insignificance of the first, while the roles of kinematic hardening and Bauschinger effect are also small but they could be important for cyclic plastic loading.

5. Appendix A

In order to find the stress distribution in a circular cross section given an applied load, the axial force and moment equilibrium are imposed. A detailed derivation is presented in this Appendix.

5.1. Elastic-perfectly plastic material: primary plastic regime, PI

The area of the circular segment that has undergone plasticity is given by

$$A_{c0} = r^2(\theta_0 - \sin\theta_0 \cos\theta_0) = r^2(\theta_0 - \sin 2\theta_0/2). \tag{26}$$

The y-position of its centroid is calculated as

$$y_{c0} = 2r\sin^3\theta_0/\left[3(\theta_0 - \sin\theta_0\cos\theta_0)\right] = 2r\sin^3\theta_0/\left[3(A_c/r^2)\right] = 2r^3\sin^3\theta_0/(3A_c)\,. \tag{27}$$

We can carry out integrations in the (r, θ) polar coordinates such that $y = r\cos\theta$. The stress distribution in the elastic area of this regime is obtained as

$$\sigma(y) = \sigma_y \times (y + d)/c, \tag{28}$$

after imposing

$$\sigma(y = c - d) = \sigma_y \quad \text{and} \quad \sigma(y = -r) = \sigma_y \times (-r + d)/c. \tag{29}$$

Hence in polar coordinates the stress profile is calculated as

$$\sigma(\theta) = \sigma_y(r\cos\theta + d)/c. \tag{30}$$

Imposing static equilibrium in the longitudinal direction leads to

$$A_c\sigma_y + \int_{-r}^{c-d} [2r\sin\theta\sigma(y)]\,dy = N \tag{31}$$

or in polar coordinates

$$A_c\sigma_y + (2\sigma_y/c)\int_{\pi}^{\theta_0} [(r\cos\theta + d)r\sin\theta(-r\sin\theta)]\,d\theta = N \tag{32}$$

which after integration and substitution of A_c from equation (26) becomes

$$(\theta_0 - \sin 2\theta_0/2) - (2/c)\left[r\sin^3\theta_0/3 + d(\theta_0 - \sin 2\theta_0/2)/2 - \pi d/2\right] = N/(r^2\sigma_y). \tag{33}$$

Imposing momentum equilibrium leads to

$$A_c\sigma_y y_c + 2\int_{\pi}^{\theta_0} [yr\sin\theta\sigma(\theta)]\,dy = M \tag{34}$$

which after substitution of A_c from equation (26), y_c from equation (27) and $y = r\cos\theta$ and integration becomes

$$2\sin^3\theta_0/3 - (2/c)\left[-r\pi/8 + r(\theta_0 - \sin 4\theta_0/4)/8 + d\sin^3\theta_0/3\right] = M/(r^3\sigma_y). \tag{35}$$

Equation (6), (33) and (35) respectively form a set of simultaneous equations in three unknowns c, d and θ_0.

$$\begin{cases} \cos\theta_0 = (c-d)/r \\ \pi d/c + (\theta_0 - \sin 2\theta_0/2)(1 - d/c) - (2r/3c)\sin^3\theta_0 = N/(r^2\sigma_y) \\ \pi r/4c + 2(1-d/c)\sin^3\theta_0/3 - (r/4c)(\theta_0 - \sin 4\theta_0/4) = M/(r^3\sigma_y) \end{cases} \tag{36}$$

Solving the first of these equations for d and substituting in the second and the third, and then eliminating d, we have

$$\begin{cases} (\pi - \theta_0 + \sin 2\theta_0/2)\cos\theta_0 + 2\sin^3\theta_0/3 = [\pi - N/(r^2\sigma_y)]\,(c/r) \\ (\pi - \theta_0 + \sin 4\theta_0/4)/4 + 2\sin^3\theta_0\cos\theta_0/3 = [M/(r^3\sigma_y)]\,(c/r) \end{cases} \tag{37}$$

c/r can now be eliminated from one of the above equations, leading to a

single equation depending only the unknown θ_0.

5.2. Elastic-perfectly plastic material: secondary plastic regime, PII

The areas of the two circular segments are respectively given by

$$A_{c1} = r^2(\theta_1 - \sin 2\theta_1/2) \quad \text{and} \quad A_{c2} = r^2(\theta_2 - \sin 2\theta_2/2) \tag{38}$$

and the y-position of their centroids is respectively calculated as

$$y_{c1} = 2r^3 \sin^3\theta_1/(3A_{c1}) \quad \text{and} \quad y_{c2} = 2r^3 \sin^3\theta_2/(3A_{c2}). \tag{39}$$

The boundaries between elastic and plastic deformation on the two sides of the beam are

$$\cos\theta_1 = (c-d)/r \quad \text{and} \quad \cos\theta_2 = (c+d)/r = \cos\theta_1 + 2d/r. \tag{40}$$

Imposing static equilibrium in the longitudinal direction leads to

$$A_{c1}\sigma_y - A_{c2}\sigma_y + \int_{-c-d}^{c-d} [2r\sin\theta\sigma(y)]\, dy = N \tag{41}$$

which, after substituting the expressions for the circular segment areas (38), equation (40) and carrying out the integration, becomes:

$$(\theta_1 - \frac{1}{2}\sin 2\theta_1) - (\theta_2 - \frac{1}{2}\sin 2\theta_2) - \frac{4}{3}\frac{\sin^3\theta_1 - \sin^3\theta_2}{\cos\theta_1 + \cos\theta_2} + \frac{\cos\theta_1 - \cos\theta_2}{\cos\theta_1 + \cos\theta_2}(\pi - \theta_1 - \theta_2) + \\ + \frac{1}{2}\sin 2\theta_1 + \frac{1}{2}\sin 2\theta_2 = n. \tag{42}$$

Imposing the momentum equilibrium leads to

$$A_{c1}\sigma_y y_1 - A_{c2}\sigma_y t_2 + \int_{-c-d}^{c-d} [2r\sin\theta y\sigma(y)]\, dy = M \tag{43}$$

which after integrating and substituting equations (38), (39) and (40) into the above equation becomes

$$2\sin^3\theta_1/3 + 2\sin^3\theta_2/3 - (2/c)\left\{d(\sin^3\theta_1 - \sin^3\theta_2)/3 - r\left[-4(\theta_1+\theta_2-\pi) + \sin 4\theta_1 + \sin 4\theta_2\right]/32\right\} = M/(r^3\sigma_y). \tag{44}$$

5.3. Nonlinear hardening model: stress distribution

By assuming an nonlinear material with hyperbolic hardening, the stress distribution in the cross section takes the form of $\sigma(\epsilon) = (B\epsilon + D)/(A - \epsilon)$. Imposing that $\sigma(d) = 0$ and $\sigma(c - d) = \sigma_y$ leads to

$$\sigma(y) = \frac{B(\epsilon_y/c)(y+d) + D}{A - (\epsilon_y/c)(y+d)} \tag{45}$$

The mathematical description of the stress distribution in polar coordinates is obtain by substituting $y = r\cos\theta$ into (45)

$$\sigma(\theta) = \frac{B(\epsilon_y/c)(r\cos\theta + d) + D}{A - (\epsilon_y/c)(r\cos\theta + d)}. \tag{46}$$

Al-Qureshi, H., 1999. Elastic-plastic analysis of tube bending. International Journal of Machine Tools and Manufacture 39 (1), 87–104.

Association, B. S. S., nd. Comparison of structural design in stainless steel and carbon steel. http://www.bssa.org.uk/topics.php?article=125, accessed: 2015-11-16.

Baragetti, S., 2006. A theoretical study on nonlinear bending of wires. Meccanica 41 (4), 443–458.

Bonfanti, A., Bhaskar, A., 2015. Elastoplastic response and recoil of honeycomb lattices. Proceeding A Submitted.

Chakrabarty, J., 2006. Theory of plasticity. Butterworth-Heinemann.

Chun, B. S., Lim, H.-S., Sagong, M., Kim, K., 2004. Development of a hyperbolic constitutive model for expanded polystyrene (eps) geofoam under triaxial compression tests. Geotextiles and Geomembranes 22 (4), 223–237.

Dafalias, Y., Popov, E., 1975. A model of nonlinearly hardening materials for complex loading. Acta Mechanica 21 (3), 173–192.

Dharmasena, K. P., Wadley, H. N., Xue, Z., Hutchinson, J. W., 2008. Mechanical response of metallic honeycomb sandwich panel structures to high-intensity dynamic loading. International Journal of Impact Engineering 35 (9), 1063–1074.

El-Domiaty, A., Elsharkawy, A., 1998. Stretch-bending analysis of u-section beams. International Journal of Machine Tools and Manufacture 38 (1), 75–95.

Fare, S., Ge, Q., Vedani, M., Vimercati, G., Gastaldi, D., Migliavacca, F., Petrini, L., Trasatti, S., 2010. Evaluation of material properties and design requirements for biodegradable magnesium stents. Materia (Rio de Janeiro) 15 (2), 96–103.

Gibson, L., Ashby, M., Schajer, G., Robertson, C., 1982. The mechanics of two-dimensional cellular materials. In: Proceedings of the Royal Society of London A: Mathematical, Physical and Engineering Sciences. Vol. 382. The Royal Society, pp. 25–42.

Gibson, L. J., Ashby, M. F., 1999. Cellular solids: structure and properties. Cambridge university press.

Johnson, W., Mellor, P. B., 1983. Engineering plasticity. E. Horwood.

Kaliszky, S., 1989. Plasticity: theory and engineering applications. Elsevier Amsterdam.

Miller, J., Kyriakides, S., Bastard, A., 2001. On bend-stretch forming of aluminum extruded tubes–I: experiments. International Journal of Mechanical Sciences 43 (5), 1283–1317.

Mines, R., Jones, N., 1995. Approximate elastic-plastic analysis of the static and impact behaviour of polymer composite sandwich beams. Composites 26 (12), 803–814.

Prager, W., Hodge, P. G., 1951. Theory of perfectly plastic solids. Mathematical Association of America.

Rajani, B., 2012. Nonlinear stress–strain characterization of cast iron used to manufacture pipes for water supply. Journal of Engineering Materials and Technology 134 (4), 041005.

Rasmussen, K. J., 2003. Full-range stress–strain curves for stainless steel alloys. Journal of constructional steel research 59 (1), 47–61.

Rees, D., 2006. Basic engineering plasticity: An introduction with engineering and manufacturing applications. Butterworth-Heinemann.

Saje, M., Turk, G., Kalagasidu, A., Vratanar, B., 1998. A kinematically exact finite element formulation of elastic–plastic curved beams. Computers & structures 67 (4), 197–214.

Samuel, K., 2006. Limitations of hollomon and ludwigson stress–strain relations in assessing the strain hardening parameters. Journal of Physics D: Applied Physics 39 (1), 203.

Štok, B., Halilovič, M., 2009. Analytical solutions in elasto-plastic bending of beams with rectangular cross section. Applied Mathematical Modelling 33 (3), 1749–1760.

Tian, J., Kim, T., Lu, T., Hodson, H., Queheillalt, D., Sypeck, D., Wadley, H., 2004. The effects of topology upon fluid-flow and heat-transfer within cellular copper structures. International Journal of Heat and Mass Transfer 47 (14), 3171–3186.

Tian, J., Lu, T., Hodson, H., Queheillalt, D., Wadley, H., 2007. Cross flow heat exchange of textile cellular metal core sandwich panels. International journal of heat and mass transfer 50 (13), 2521–2536.

Tuncer, E., 2005. Numerical calculations of effective elastic properties of two cellular structures. Journal of Physics D: Applied Physics 38 (3), 497.

Wadley, H., Dharmasena, K., Chen, Y., Dudt, P., Knight, D., Charette, R., Kiddy, K., 2008. Compressive response of multilayered pyramidal lattices during underwater shock loading. International Journal of Impact Engineering 35 (9), 1102–1114.

Xu, Y., Zhang, L., Yu, T., 1987. The elastic-plastic pure bending and springback of l-shaped beams. International journal of mechanical sciences 29 (6), 425–433.

Yang, S., Leong, K.-F., Du, Z., Chua, C.-K., 2001. The design of scaffolds for use in tissue engineering. part i. traditional factors. Tissue engineering 7 (6), 679–689.

Yang, S., Leong, K.-F., Du, Z., Chua, C.-K., 2002. The design of scaffolds for use in tissue engineering. part ii. rapid prototyping techniques. Tissue engineering 8 (1), 1–11.

Yu, T., Johnson, W., 1982. Influence of axial force on the elastic-plastic bending and springback of a beam. Journal of Mechanical Working Technology 6 (1), 5–21.

Zhao, J., Zhai, R., Qian, Z., Ma, R., 2013. A study on springback of profile plane stretch–bending in the loading method of pretension and moment. International Journal of Mechanical Sciences 75, 45–54.